JMEPEG (2012) 21:2195–2202
DOI: 10.1007/s11665-012-0151-1

1059-9495/$19.00

Effect of NaOH on the Structure and Corrosion Performance of Alumina and Silica PEO Coatings on Aluminum

D. Salehi Doolabi, M. Ehteshamzadeh, and S.M.M. Mirhosseini

(Submitted November 20, 2010; in revised form December 30, 2011)

The effect of NaOH content of electrolyte on the properties of ceramic coatings, produced in silicate solution, was studied. Morphology, chemical analysis, phase composition, and cross-section of the ceramic coatings were investigated by SEM, EDS, XRD, and OM, respectively. The corrosion resistance and corrosion mechanism were also studied using potentiodynamic polarization and electrochemical impedance spectroscopy in a 3.5% NaCl solution. To study the surface roughness, a brightness SEM image analysis method was used. Results suggested that increasing the NaOH concentration of sediment production size causes thickness and coating roughness to decrease. The lowest corrosion rate belonged to the twofold layer coating produced in 10 g/L of NaOH. Other samples, with higher concentrations of NaOH, had reduced porosity, and thus an increase in the corrosion resistance was observed. These coatings mainly consisted of α/γ-Al_2O_3 and amorphous silica.

Keywords ceramic coating, EIS, NaOH, plasma electrolytic, roughness

1. Introduction

Plasma electrolytic oxidation (PEO) is an advanced coating technique, developed during the past two decades. PEO is used widely to coat light alloys and even some composites, such as SiCp/A356 with ceramic oxide layers (Ref 1-3). This technique has been developed because of its special advantages, such as a high coating deposition rate, and the ability to coat substrates of different shapes and sizes (Ref 4-6).

Due to the impressive abrasive, cohesive, erosive, corrosive, electrical and even thermal properties, PEO coatings have found a wide range of applications in various industries (Ref 4, 7). Various types of layers, from completely porous to extremely dense, can be formed on aluminum parts by means of PEO (Ref 7-9). Properties (Ref 1, 4), formation mechanisms (Ref 10, 11), simulation (Ref 12), and phase composition, as well as contribution of oxide layers on aluminum alloys, have been extensively reported in previous literature.

Silicate-containing electrolytes are commonly used in PEO to form oxide layers on aluminum. By addition of these compounds, the oxide deposition rate increases and aluminosilicate phases come into final coatings. These phases are normally not as hard as alumina polymorphs and significantly reduce the hardness and embrittlement of coatings (Ref 4, 10). Furthermore, because silicate phases have a lower thermal conductivity than alumina, silicate-containing coatings present better thermal shock resistance and can be used as thermal barrier coatings (TBCs). The coating properties are heavily influenced by processing parameters such as electrolyte composition, concentration, pH, type and density of applied current, as well as chemical composition of the substrate (Ref 4, 10, 13). Among these factors, electrolyte composition and concentration are the two most important factors. For instance, an increase in Si content of the electrolyte enhances the growth rate of the coating in silicate electrolytes, but also promotes the formation of softer aluminasilicate phase (Al-Si-O) in the coating (Ref 14). The addition of inorganic salt ($Na_2WO_4{\cdot}2H_2O$) to the electrolyte marginally increases the ratio of the thickness of internal dense layer to the total coating thickness, while the coating deposition rate decreases (Ref 10). The film growth rate decreases significantly with increasing electrolyte concentration from 0.5 to 2 g/L KOH, since the rate of anodic dissolution increases (Ref 13). Coatings produced in silicate electrolyte have a more homogeneous morphology than those produced in phosphate electrolyte. Silicon atoms locate mainly in the outer region of the coating, while phosphorus atoms distribute homogeneously across the coating (Ref 15). A white layer was formed on aluminum alloy surface in $(NaPO_3)_6$ and Na_2SiO_3 solution. Also, it was shown after addition of 6 g/L NH_4VO_3 to the electrolyte that a black ceramic layer was formed (Ref 16).

It should be mentioned that PEO is a technique to produce hard and thick ceramic coatings on metals, such as aluminum, titanium, magnesium, niobium and their alloys for applications needing high temperature, wear, and corrosion resistance. This technique is usually carried out in alkaline solutions (Ref 4, 16-19). However, there is not enough information about the effect of NaOH concentration in electrolyte on the microstructure and corrosion performance of the PEO coatings. In this work, the effect of NaOH concentration on the morphology, thickness,

D. Salehi Doolabi and **M. Ehteshamzadeh**, Department of Materials Science and Engineering, Faculty of Engineering, Shahid Bahonar University of Kerman, P.O. Box 76175-133, Islamic Republic Blvd., Kerman, Iran; and **S.M.M. Mirhosseini,** Faculty of Materials Science and Engineering, Sharif University of Technology, Tehran, Iran. Contact e-mail: ehtesham@mail.uk.ac.ir.

microstructure, and corrosion behavior of the silicate-containing oxide layer on commercially pure aluminum was presented.

2. Experimental Procedures

Rectangular coupons ($1 \times 30 \times 25$ mm^3) of commercially pure aluminum were used as substrates; the chemical composition was 0.44% Fe, 0.22% Si, 0.09% Cu, 0.03% Mn, and Al balance. After polishing on SiC abrasive paper up to grit number 1200, samples were degreased using a NaOH diluted aqueous solution and then washed by acetone and distilled water.

Electrolytes were prepared by dissolving of different amount of NaOH (10, 20, 30, and 40 g/L) and constant amount of Na_2SiO_3 (30 g/L) in distilled water (all chemicals were analytical grade). The samples served as the anode in the electrolysis process and a predefined DC voltage (500 V) was applied for 1 min (Table 1). The electrolyte was stirred during the process using a magnetic stirrer to avoid raising the electrolyte temperature next to the sample. After coating, samples were washed using distilled water and then dried in air. After macroscopic study of the samples, their centers (10×10 mm^2) were cut by microcutter and used for further investigation.

The phase composition of the coatings was studied using a Philips X-ray diffract meter with a step size equal to 0.02° in the range from 5° to 110°. The morphological features of the samples were obtained by a scanning electron microscope, (SEM, CAMSCAN 2300 MV equipped with an energy dispersive X-ray spectrometer (EDS), with a beam energy of 25.0 kV). Surface roughness (R_a) was measured using SEM, and then it was compared with results obtained by RUGOSURF (Brown & Sharp) surface roughness tester.

In this technique, the darkness and brightness of SEM micrographs in the secondary electron (SE) beam mode, as a function of its gray levels, was calibrated and reported as roughness of the samples surface. If the gray levels are interpreted as an elevation in a representation of the surface image, texture can be replaced with roughness. The well-known difficulties with stating a precise definition of surface roughness explains the difficulties with defining the texture as well (Ref 20).

Using a SEM micrograph photo analyser, roughness of the top oxide layer was obtained on a 600-μm line for a fixed magnification of 280. This measurement was taken three times for more accuracy.

In the next step, five samples were cut across their thickness, mounted, and finally polished using SiC abrasive papers up to grit number 4000. These samples were used for obtaining the thickness of the oxide layer using an optical microscope. The microhardness profile across the film was measured using a Struers Model DURAMIN20 Vickers microhardness tester under 50 g load and 10 s duration.

Potentiodynamic polarization and electrochemical impedance spectroscopy (EIS) techniques were employed to study the corrosion behavior of the coatings in a 3.5% NaCl solution, using a PARC EG&G Model 263A potentiostat coupled with a PC14 controller. A three-electrode cell was used, consisting of a saturated calomel electrode (SCE), a platinum foil counter electrode and a specimen as a working electrode with a surface area of 1 cm^2. A Luggin capillary with a porous tip was employed to minimize the contamination and prevent potential variations in the reference electrode, as well as positioning it in the desired point in the cell. Potentiodynamic polarization curves were recorded in a near complete range of potential around the open circuit potential at a sweep rate of 2 mV/s. The results were analyzed using "Softcorr352" software. EIS measurements were carried out using a 10-mV sinusoidal perturbation applied in the 100 kHz to 10 mHz frequency range with 30 steps per decade. The spectra were analyzed in terms of an equivalent circuit using "ZView2" software. To verify data reproducibility, each measurement was carried out for three specimens treated under the same conditions and the mean values were reported.

3. Results

Morphology of the samples in Fig. 1 shows that raising the NaOH concentration results in a smaller number and better splitting of surface hills around the sample.

Table 2 and Fig. 2 illustrate the effect of the addition of NaOH on the relative decrease in roughness (R_a) and increase in the number of micro-cracks of the top oxide layer, respectively. In addition, Table 2 shows that the results obtained from image analysis (SEM) are in good agreement with data of surface roughness tester.

Optical image cross-sections of grown oxide layers are illustrated in Fig. 3. Generally, it shows that by addition of NaOH, the thickness of the oxide layer are reduced (Table 1) and the final coatings simultaneously gets denser. However, Sample one has unique characteristics, due to having the thickest oxide layer as well as having two completely distinguished sub-layers which are formed on each other.

Microhardness profile of coating cross-section gradually increases from the interior layer (600-900 HV) to outer layer (1000-1200 HV), and with the addition of NaOH, the hardness of coating increases. Figure 4 is illustrated as an example for the cross-section microhardness profile of coating samples 2, 4.

EDS analysis of the top oxide layers, as a function of NaOH concentration, are shown in Fig. 5. It is clearly seen that as a result of more NaOH in electrolyte, Al is concentrated in top oxide layers and the partial fraction of Si decreases simultaneously.

The XRD pattern of sample 2 is shown in Fig. 6. The minimum of the second derivative was applied to find the position and intensity of XRD peaks for more accuracy. Using this method accompanied with overlapping peaks gives optimal results.

Table 1 Plasma electrolysis conditions

Sample no.	Concentration, g/L	I_{Start}, A/cm^2	I_{Finish}, A/cm^2	Thickness, μm
1	30 g/L Na_2SiO_3 + 10 g/L NaOH	0.63	0.35-0.41	26.3-28.8
2	30 g/L Na_2SiO_3 + 20 g/L NaOH	0.67	0.27-0.38	25-27.2
3	30 g/L Na_2SiO_3 + 30 g/L NaOH	0.76	0.31-0.39	19.9-23.6
4	30 g/L Na_2SiO_3 + 40 g/L NaOH	0.82	0.36-0.40	13.2-17.3

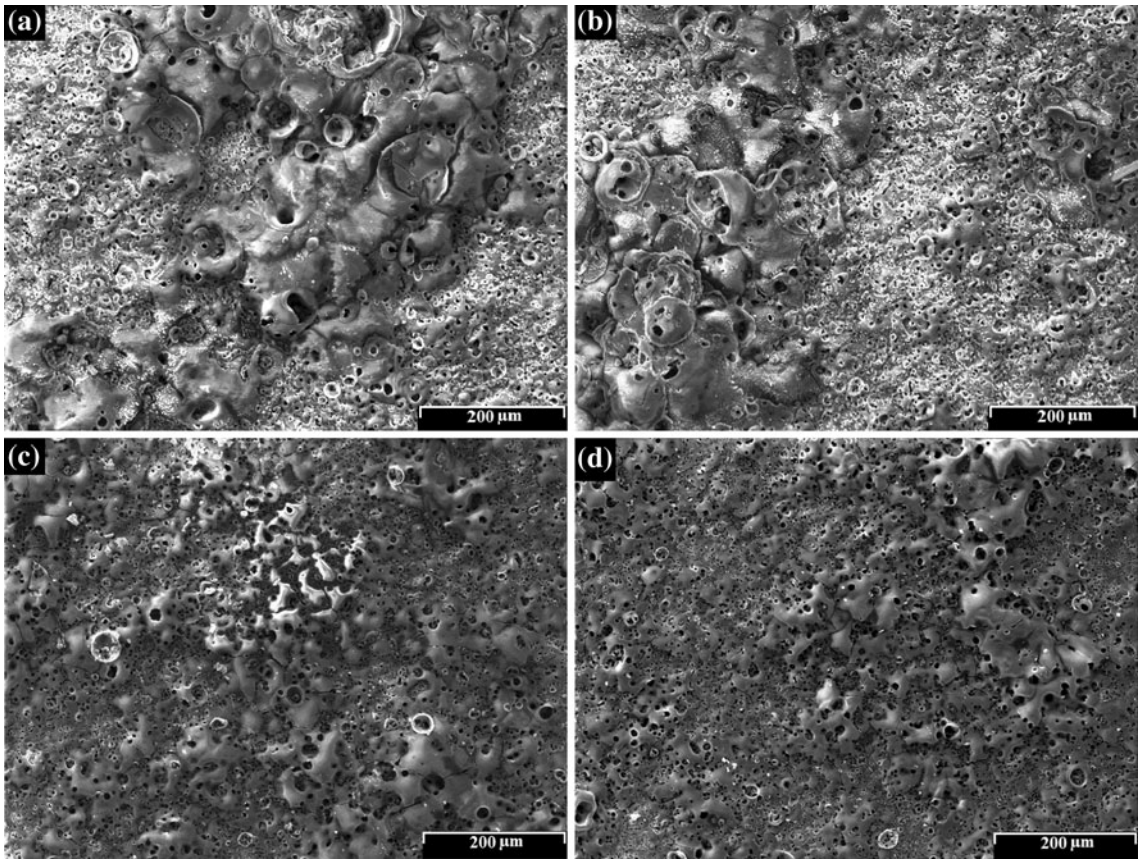

Fig. 1 Micrographs of the coatings produced in the silicate solution containing different concentrations of NaOH: (a) 10 g/L, (b) 20 g/L, (c) 30 g/L, and (d) 40 g/L

Table 2 Roughness R_a of the coatings prepared in different concentrations of NaOH (by SEM and roughness tester)

NaOH concentration, g/L	Line length, µm	R_a by SEM, µm	Magnification	R_a by surface roughness tester, µm
10	584.1	1.13	286×	1.21
20	619.8	1.08	275×	1.15
30	631	0.92	267×	1.01
40	576.4	0.84	285×	0.92

The broad peak, located between 22° and 24° in Fig. 6, provides evidence of the existence of silica-based compounds in final oxide layers. In order to make this peak clear, *Y*-axis is laid out as the square root intensity. In addition, for easier and more accurate identification of the crystalline phase, the background pattern has been subtracted from the original pattern.

Al peaks in XRD spectra are related to the substrate; the main crystalline phases of coating are α/γ-Al_2O_3, and Al_2SiO_5. Moreover, SiO_2 (in the form of crystoballite and tridimite which are polymorphs of silica) and even mullite (which is an intermediate solid solution) are involved in top layer, although, as minor phases.

Polarization curves of samples are presented in Fig. 7 and derived results from these curves are listed in Table 3. According to these curves, sample one represented the minimum corrosion rate and its curve also had the sharpest anodic branch in comparison with the others. It is clearly seen that by adding more than 20 g/L of NaOH to the electrolyte, corrosion rate of the samples decreased.

Figure 8 represents EIS results in the form of Nyquist, Bode-phase, and Bode plots. It is clear that the Nyquist curve of sample one is completely different from the others. Distinguishing characteristics of this sample are due to its lack of semi-inductive behavior in other samples, and also having two completely separate capacitance loops.

4. Discussion

4.1 Morphological Study

4.1.1 Distribution of Precipitations and Roughness. By increasing of the NaOH concentration, the following reaction is enhanced:

$$4OH^- \rightarrow O_2 \uparrow + 2H_2O + 4e^- \quad \text{(Eq 1)}$$

Excessive oxygen and electrons that are produced in this reaction result in a thicker vapor shield and the existence of

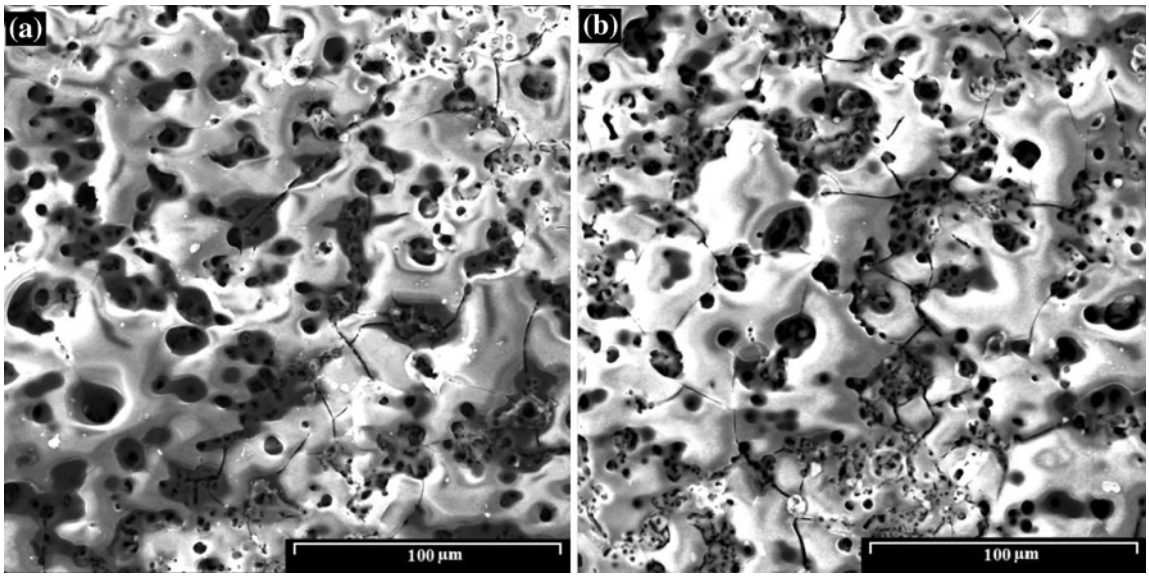

Fig. 2 Cracks in the coatings produced in the silicate solution containing different concentrations of NaOH: (a) 30 and (b) 40

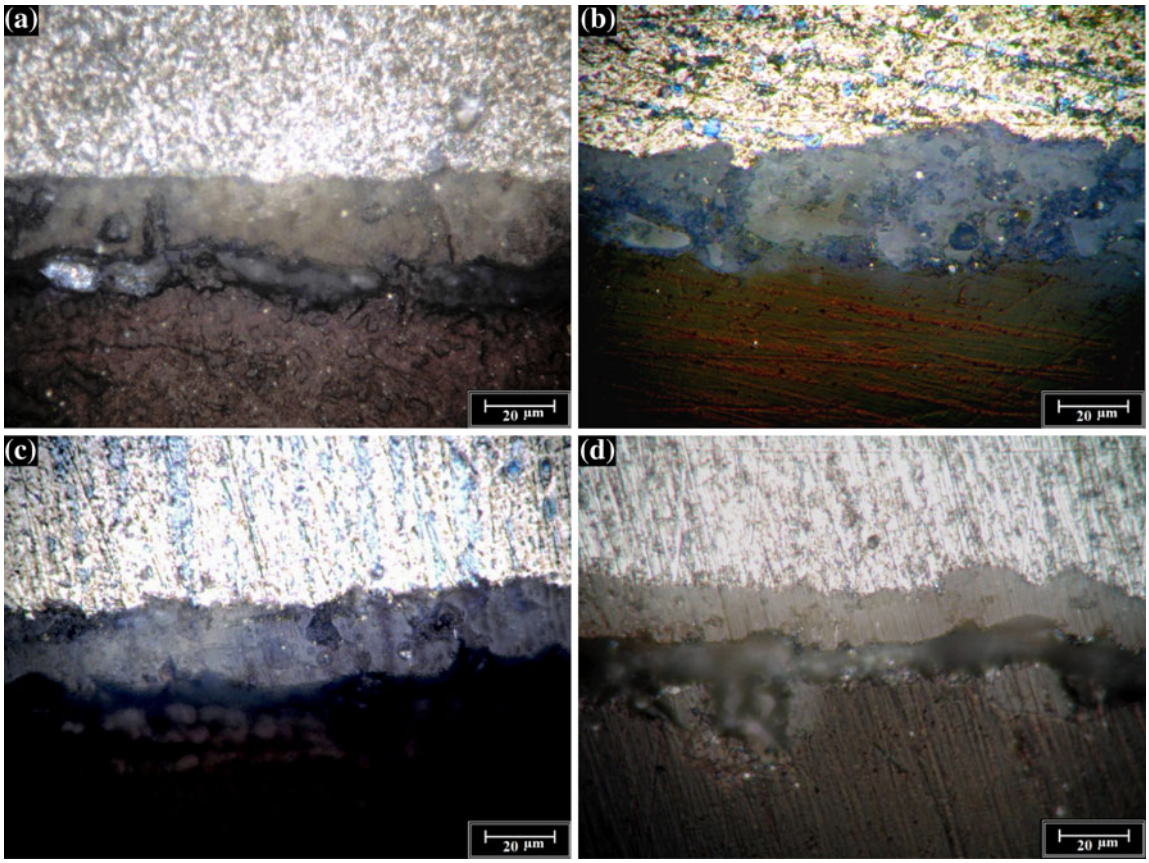

Fig. 3 Optical microscopy image of cross section of ceramic coating product in silicate solution contains different concentrations of NaOH: (a) 10 g/L, (b) 20 g/L, (c) 30 g/L, and (d) 40 g/L

more discharge around the samples, respectively. More oxygen release and a greater difference between the sample's surface temperature and boiling point of the surrounding solution make the vapor layer around the sample change from an unstable shield to a continuous one (Ref 21, 22). Simultaneous occurrence of these two effects leads to a better distribution of sparks all around the sample and a decreased in roughness of the final coatings.

4.1.2 Surface Cracks. The following reasons are claimed to be responsible for more micro-cracks on the top oxide layer:

(a) The coating's internal normal or shear stresses can induce intrinsic, thermal, or structural tensions. Relaxation of these stresses usually appears as a network of internal and external cracks on the final coating (Ref 16).

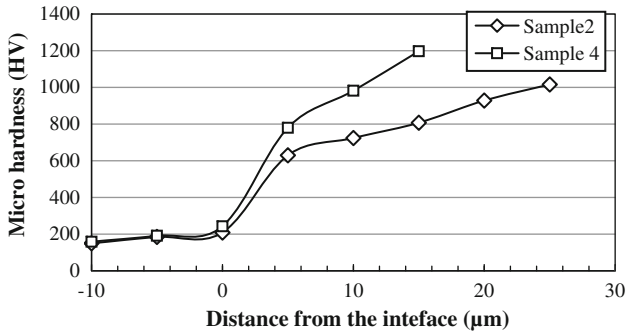

Fig. 4 Variations in cross-section microhardness of coatings for samples 2, 4 as a function of the distance from the interface

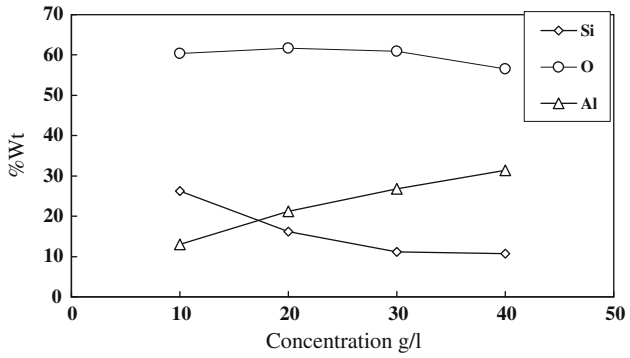

Fig. 5 Changes in the chemical analysis of surface coatings, caused by EDS, is proportioned to different concentrations of NaOH

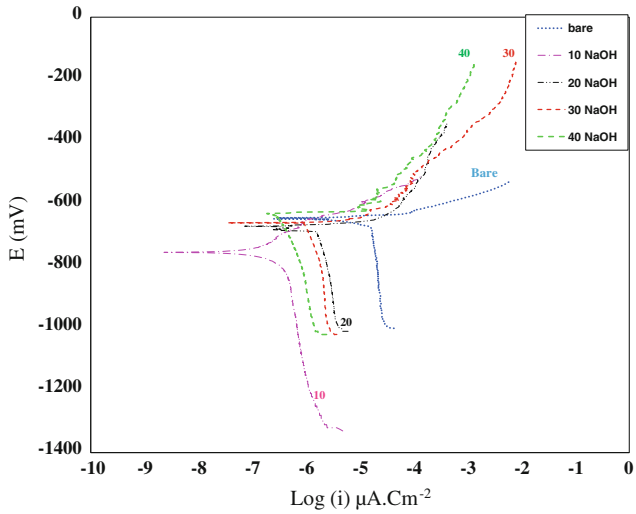

Fig. 7 Polarization plots of ceramic coatings produced in different concentrations of NaOH: (a) 10 g/L, (b) 20 g/L, (c) 30 g/L, and (d) 40 g/L

Table 3 Potentiodynamic polarization parameters of the coatings prepared in different concentrations of NaOH

NaOH concentration, g/L	OCP, mV	I_{corr}, nA	β_a (V/decade)	β_c (V/decade)
Bare	−646.4	11,930	4.09E−02	6.38E−01
10	−754.3	57.61	7.08E−02	5.77E−02
20	−674.3	2852	2.36E+02	9.60E−02
30	−661.3	2121	9.21E−02	4.47E+01
40	−635.3	750	8.93E−02	5.52E+00

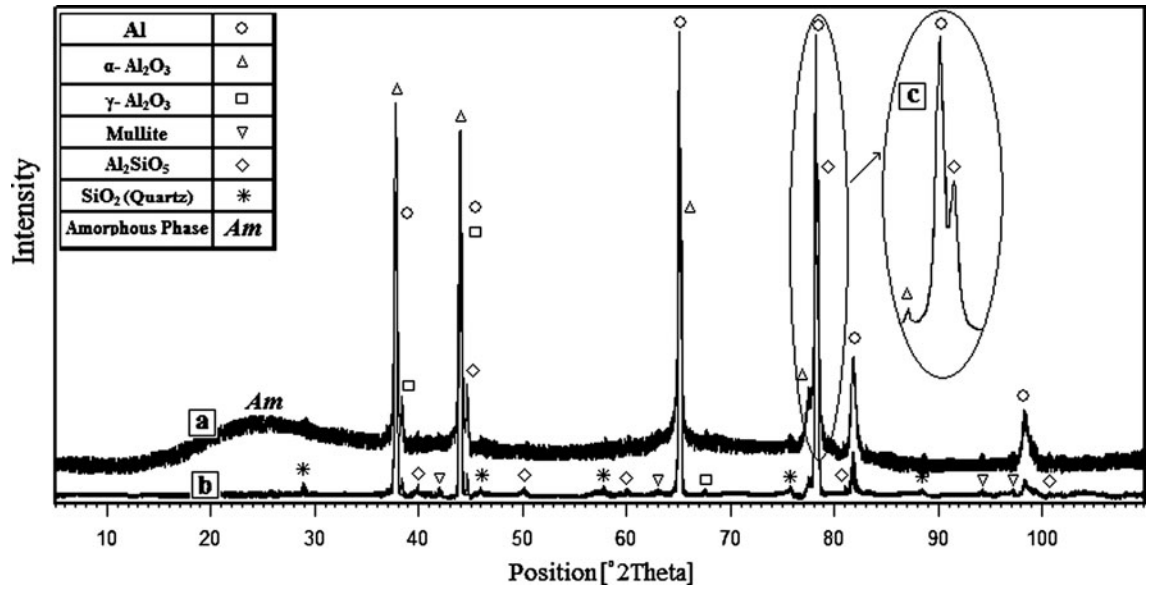

Fig. 6 X-ray diffraction pattern of the coating produced in silicate solution containing 20 g/L NaOH (sample 2): (a) *Y*: square root of the peak intensity, (b) subtraction of the background pattern and the original pattern, and (c) typical overlap of the crystalline phase peaks

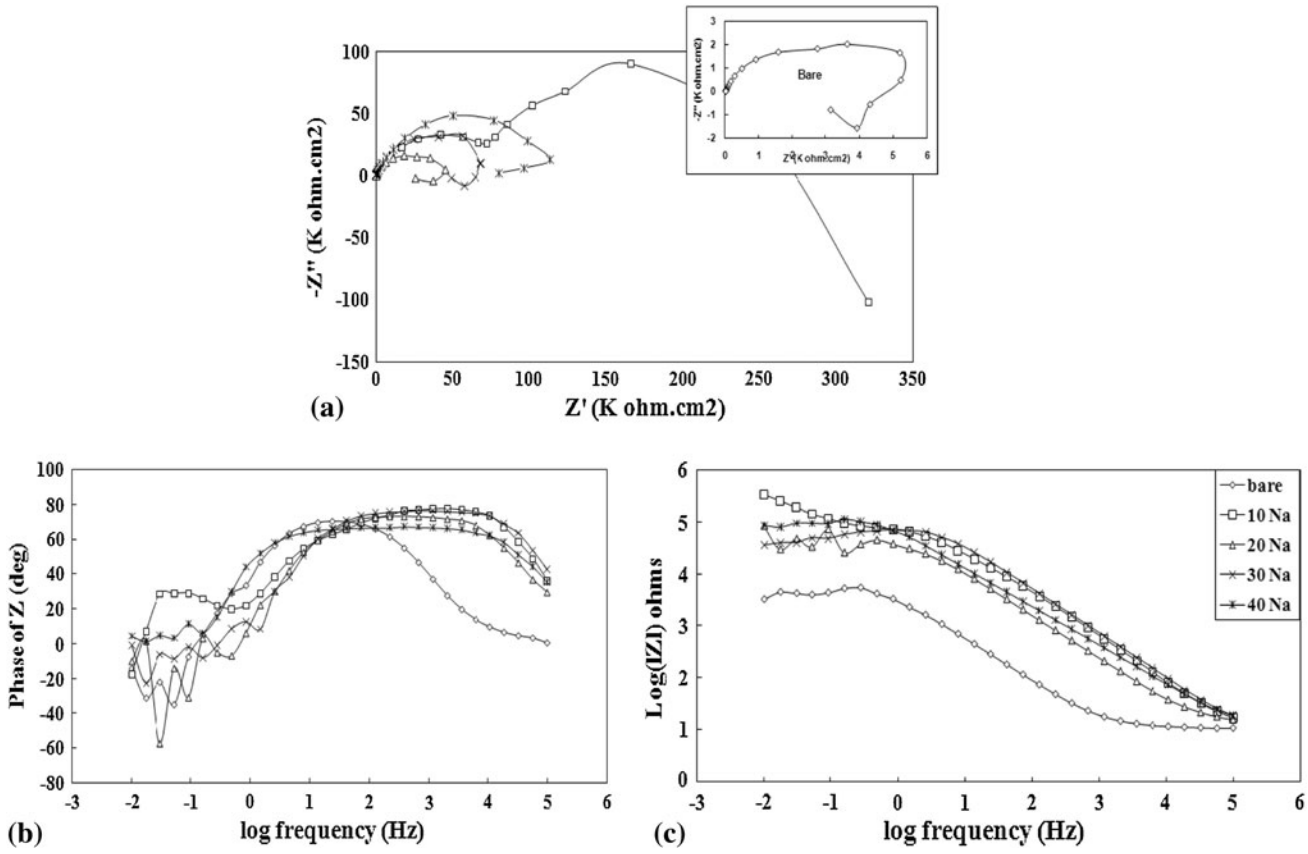

Fig. 8 EIS plots of ceramic coatings prepared in different concentrations of NaOH: (a) Nyquist, (b) Bode-Phase and (c) Bode

(b) Solidification shrinkage in the fusion zone, at the end of discharge channels, results in holes and shrinking defects on top oxide layer. These defects finally lead to micro-cracks at their tips (Ref 7).

(c) Due to rapid solidification, the top layer of these coatings usually consists of brittle and unstable phases (Ref 23). Moreover, the external oxide layer usually has a greater elastic coefficient and more residual stress (Ref 24). Also, microhardness investigation across the coating showed that the average hardness of the outer layer is more than that of inner layer of coating. This causes the formation of micro-cracks as a result of stress relaxation concentrated on the top oxide layer.

4.2 Coatings Cross-Section

The thickness of the oxide layer decreases with increasing NaOH concentration due to these two reasons: (1) rapid chemical and electrochemical dissolution of the coatings and substrate and secondary dissolution of oxide layer (Ref 13), as well as (2) the increasing ionic ratio of OH^-/SiO_3^{2-} and pH in electrolyte. These two reasons cause reaction 1 to occur more rapidly than reaction 2 and result in decreasing the rate of precipitation of silicate-containing phases. In this regard, the rate of coating formation reduces drastically (Ref 14).

$$SiO_3^{2-} + 2H^+ + (n-1)H_2O \rightarrow SiO_2 \cdot nH_2O \qquad \text{(Eq 2)}$$

Also, common reduction reactions occure to supply electron neutrality, such as hydrogen evolution reaction (HER).

Large amounts of heat, as a result of discharges, work as an annealing medium for these coatings (Ref 7). It should be noted that these heat-affected zones are much larger than the diameter of each discharge channel. Therefore, annealing affects the entire coating thickness, whereas, micro-cracks are concentrated in the top oxide layer.

4.3 Chemical and Phase Analysis

By addition of NaOH to the electrolyte, reaction 1 occurs rapidly in contrast with reaction 2. The Al fraction in final coating increases while the Si concentration decreases. Reaction 1, in effect, releases more O_2 and causes dissolution of the substrate. This leads to surpassing the oxidation of Al; and therefore, Al concentration in the final coating is surpassed.

However, there are two challenges in identifying the effect of NaOH concentration on the contribution of each phase in final coatings: (1) overlapping of the peaks of the Al substrate, α-Al_2O_3, γ-Al_2O_3, and Al_2SiO_5, particularly at $2\theta = 37.75°$, 43.96°, 65°, and 78.18° (Fig. 6c); (2) various compositions of amorphous phases in each sample.

It should be noted that although the Gibbs free energy of formation of mullite from Al_2O_3 and SiO_2 is much lower than these two phases, due to the low precipitation time in this process, crystalline Al_2O_3 and amorphous SiO_2 are more likely to form instead of mullite.

4.4 Polarization and EIS Analysis

The difference between the EIS curve in sample one (specially Nyquist) in Fig. 8a, and other samples can be

attributed to the twofold layer characteristics of coatings formed on this sample (see a cross-section of this sample in Fig. 3).

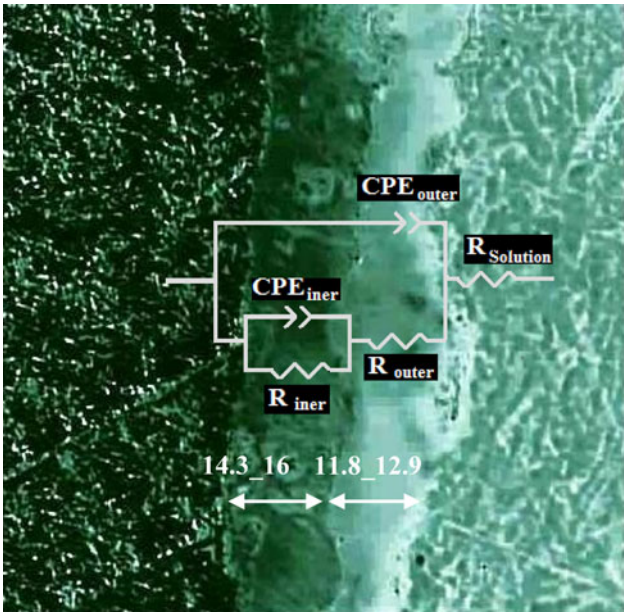

Fig. 9 Equivalent circuit of sample one (the coating prepared in 30 g/L Na_2SiO_3 + 10 g/L NaOH)

According to results of polarization tests (Fig. 7 and Table 3), increasing the amount of NaOH in the electrolyte to more than 20 g/L reduces the porosities and also increases the corrosion resistance of the samples. Equivalent circuits of electrochemical reactions for samples 2, 3, and 4 were so unreliable that they were analyzed several times for accuracy. But the equivalent circuit suggested for sample one (Fig. 9) was reliable enough.

The existence of two CPE coefficients in this sample comes from a coating with double-layer characterization.

R_1 and CPE_1, which are related to high frequency, can refer to a porous external layer; R_2 and CPE_2, which are calculated in low frequencies, comes from an internal dense layer (Ref 25). Table 4 lists the obtained results from the curves presented in Fig. 9.

Results of fitting the data obtained from the equivalent circuit are shown in Fig. 9, and the electrochemical impedance analysis of the real data is illustrated in Fig. 10. Sample one, unlike the other coatings that all have semi-induced behavior, has two separate layers: a porous outer layer and an internal layer with less porosity.

It should be noted that the inner layer is different from a barrier layer in anodising or PEO coatings produced in galvanostatic conditions.

In fact, the inner layer thickness and porosity is larger and the electrical resistance is smaller, while in the barrier layer coatings, the resistance of R_1 to R_2 is absolutely negligible. The incomplete induction loops in the low-frequency range

Table 4 Typical fitting data for sample one (the coating prepared in 30 g/L Na_2SiO_3 + 10 g/L NaOH)

Element	$R_{Solution}$, Ω cm^2	CPE_{Outer}-T (F)	CPE_{Outer}-P	R_{Outer}, Ω cm^2	CPE_{Inner}-T (F)	CPE_{Inner}-P	R_{Inner}, Ω cm^2
Value	9.816	1.02E−06	0.84152	81,029	2.43E−05	0.87237	1.87E+05

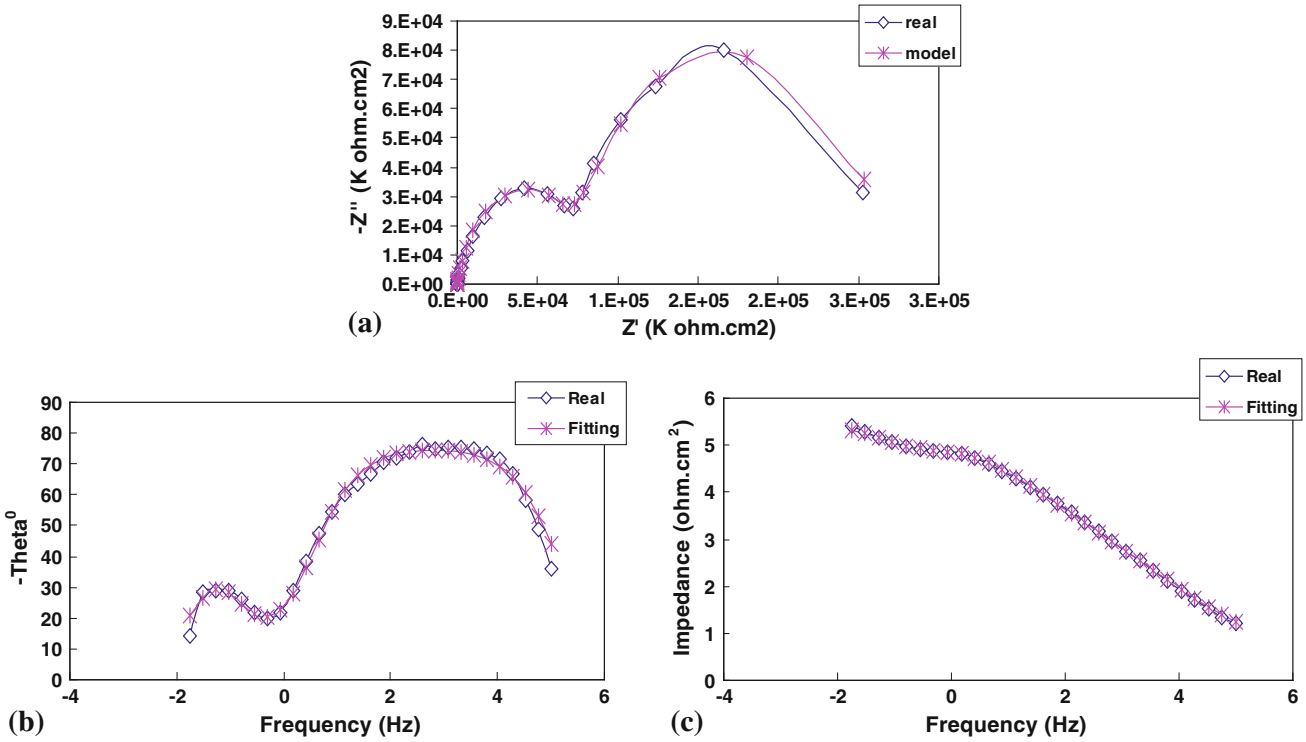

Fig. 10 Fit result of EIS plots of sample one (the coating prepared in 30 g/L Na_2SiO_3 + 10 g/L NaOH)

(Fig. 8a.) in all samples except sample one can be the outgrowth of the relaxation process of Cl^{-}_{ads} and H^{+}_{ads} ions on aluminum oxide, or the aluminum substrate (Ref 26).

5. Conclusion

1. Increasing of NaOH content of the electrolyte decreased the average roughness of the coatings as well as the coating thickness.
2. Increasing of NaOH content of the electrolyte causes an increase in aluminum and a decrease in silicon and oxygen on the surface of the coatings.
3. The coating that formed in the lowest NaOH content of the electrolyte showed the highest corrosion resistance, which could be attributed to the formation of an internal low-porosity layer.

Acknowledgment

The authors like to express their appreciation to Mr. A.R. Manshouri for edition assistance.

References

1. S. Cui, J. Han, Y. Du, and W. Li, Corrosion Resistance and Wear Resistance of Plasma Electrolytic Oxidation Coatings on Metal Matrix Composites, *Surf. Coat. Technol.*, 2007, **201**, p 5306–5309
2. W.-C. Gu, G.-H. Lv, H. Chen, G.-L. Chen, W.-R. Feng, and S.-Z. Yang, Characterization of Ceramic Coatings Produced by Plasma Electrolytic Oxidation of Aluminum Alloy, *Mater. Sci. Eng. A*, 2007, **447**, p 158–162
3. W.-C. Gu, G.-H. Lv, H. Chen, G.-L. Chen, W.-R. Feng, and S.-Z. Yang, PEO Protective Coatings on Inner Surface of Tubes, *Surf. Coat. Technol.*, 2007, **201**, p 6619–6622
4. A.L. Yerokhin, X. Nie, A. Leyland, A. Matthews, and S.J. Dowey, Plasma Electrolysis for Surface Engineering, *Surf. Coat. Technol.*, 1999, **122**, p 73–93
5. F. Monfort, A. Berkani, E. Matykina, P. Skeldon, G.E. Thompson, H. Habazaki, and K. Shimizu, Development of Anodic Coatings on Aluminium Under Sparking Conditions in Silicate Electrolyte, *Corros. Sci.*, 2007, **49**, p 672–693
6. W.-C. Gu, G.-H. Lv, H. Chen, G.-L. Chen, W.-R. Feng, G.-L. Zhang, and S.-Z. Yang, Investigation of Morphology and Composition of Plasma Electrolytic Oxidation Coatings in Systems of Na_2SiO_3-NaOH and $(NaPO_3)_6$-NaOH, *J. Mater. Process. Technol.*, 2007, **182**, p 28–33
7. J.A. Curran and T.W. Clyne, Thermo-physical Properties of Plasma Electrolytic Oxide Coatings on Aluminium, *Surf. Coat. Technol.*, 2005, **199**, p 168–176
8. X. Nie, A. Leyland, H.W. Song, A.L. Yerokhin, S.J. Dowey, and A. Matthews, Thickness Effects on the Mechanical Properties of Micro-arc Discharge Oxide Coatings on Aluminium Alloys, *Surf. Coat. Technol.*, 1999, **116–119**, p 1055–1060
9. S.V. Gnedenkova, O.A. Khrisanfovaa, A.G. Zavidnayaa, S.L. Sinebrukhova, P.S. Gordienkoa, S. Iwatsubob, and A. Matsuib, Composition and Adhesion of Protective Coatings on Aluminum, *Surf. Coat. Technol.*, 2001, **145**, p 146–151
10. G. Sundararajan and L. Rama Krishna, Mechanisms Underlying the Formation of Thick Alumina Coatings Through the MAO Coating Technology, *Surf. Coat. Technol.*, 2003, **167**, p 269–277
11. W. Xue, Z. Deng, Y. Lai, R. Chen, and J. Am, Preparation and Structure of Microarc Oxidation Ceramic Coatings Containing ZrO_2 Grown on LY12 Al Alloy, *Ceram. Soc.*, 1998, **81**(5), p 1365–1370
12. L.O. Snizhko, A.L. Yerokhin, N.L. Gurevina, D.O. Misnyankin, A. Pilkington, A. Leyland, and A. Matthewsb, A Model for Galvanostatic Anodising of Al in Alkaline Solutions, *Electrochim. Acta*, 2005, **50**, p 5458–5464
13. L.O. Snizhko, A.L. Yerokhin, A. Pilkington, N.L. Gurevina, D.O. Misnyankin, A. Leyland, and A. Matthews, Anodic Processes in Plasma Electrolytic Oxidation of Aluminum in Alkaline Solutions, *Electrochim. Acta*, 2004, **49**, p 2085–2095
14. A.A. Voevodin, A.L. Yerokhin, V.V. Lyubimov, M.S. Donley, and J.S. Zabinski, Characterization of Wear Protective Al-Si-O Coatings Formed on Al-Based Alloys by Micro-arc Discharge Treatment, *Surf. Coat. Technol.*, 1996, **86–87**, p 516–521
15. G. Lv, W. Gu, H. Chen, W. Feng, M. Latif Khosa, L. Li, E. Niu, G. Zhang, and S.-Z. Yang, Characteristic of Ceramic Coatings on Aluminum by Plasma Electrolytic Oxidation in Silicate and Phosphate Electrolyte, *Appl. Surf. Sci.*, 2006, **253**, p 2947–2952
16. J. Li, H. Cai, and B. Jiang, Growth Mechanism of Black Ceramic Layers Formed by Microarc Oxidation, *Surf. Coat. Technol.*, 2007, **201**, p 8702–8708
17. E.V. Parfenov, A.L. Yerokhin, and A. Matthews, Frequency Response Studies for the Plasma Electrolytic Oxidation Process, *Surf. Coat. Technol.*, 2007, **201**, p 8661–8670
18. W.-C. Gu, G.-H. Lv, H. Chen, G.-L. Chen, W.-R. Feng, and S.-Z. Yang, PEO protective coatings on inner surface of tubes, *Surf. Coat. Technol.*, 2007, **201**, p 6619–6622
19. G.P. Wirtz, S.D. Brown, and W.M. Kriven, Ceramic Coatings by Anodic Spark Deposition, *Mater. Manuf. Processes*, 1991, **6**, p 87–115
20. L. Wojnar, *Image Analysis*, CRC Press, Boca Raton, 1999
21. R.R. Nevyantseva, S.A. Gorbatkov, E.V. Parfenov, and A.A. Bybin, The Influence of Vapor-Gaseous Envelope Behavior on Plasma Electrolytic Coating Removal, *Surf. Coat. Technol.*, 2001, **148**, p 30–37
22. R.H.U. Khan, A.L. Yerokhin, T. Pilkington, A. Leyland, and A. Matthews, Residual Stresses in Plasma Electrolytic Oxidation Coatings on Al Alloy Produced by Pulsed Unipolar Current, *Surf. Coat. Technol.*, 2005, **200**, p 1580–1586
23. W. Xue, Z. Deng, Y. Lai, and R. Chen, Analysis of Phase Distribution for Ceramic Coatings Formed by Microarc Oxidation on Aluminum Alloy, *J. Am. Ceram. Soc.*, 1998, **81**(5), p 1365–1368
24. R.H.U. Khan, A. Yerokhin, X. Li, H. Dong, and A. Matthews, Surface Characterisation of DC Plasma Electrolytic Oxidation Treated 6082 Aluminium Alloy: Effect of Current Density and Electrolyte Concentration, *Surf. Coat. Technol.*, 2010, **205**, p 1679–1688
25. A. Ghasemi, V.S. Raja, C. Blawert, W. Dietzel, and K.U. Kainer, Study of the Structure and Corrosion Behavior of PEO Coatings on AM50 Magnesium Alloy by Electrochemical Impedance Spectroscopy, *Surf. Coat. Technol.*, 2008, **202**, p 3513–3518
26. S.S. Abd El Rehim, H.H. Hassan, and M.A. Amin, Corrosion Inhibition Study of Pure Al and Some of Its Alloys in 1.0 M HCl Solution by Impedance Technique, *Corros. Sci.*, 2004, **46**, p 5–24